ACS OMEGA

http://pubs.acs.org/journal/acsodf

Article

Morphological, Thermal, and Mechanical Properties of Electrospun Recycled Poly(ethylene terephthalate)/Graphene Oxide Composite Nanofiber Membranes

Koena Selatile, Suprakas Sinha Ray,* Vincent Ojijo, and Rotimi Emmanuel Sadiku

Cite This: *ACS Omega* 2021, 6, 21005−21015

Read Online

ACCESS | Metrics & More | Article Recommendations

ABSTRACT: This study investigates the influence of graphene oxide (GO) on the properties of electrospun recycled poly(ethylene terephthalate) (rPET) composite nanofiber membranes. GO nanosheet layers, with good hydrophilic properties, were incorporated at various loadings (0−8 wt %) during electrospinning. The surface morphological analysis revealed that GO loadings of less than 0.5 wt % lead to smoother fiber surfaces due to less agglomeration, as shown by the scanning electron microscope images. The smooth fiber surface shows that the nanosheets are intact within the rPET polymer matrix at low GO loadings. The differential scanning calorimetry results reveal that nucleation increases linearly with GO content as observed by the change in crystallization peak temperature (T_c) of rPET from 184 to 200 °C. Both the T_c and characteristic rPET crystallization peak in the X-ray diffraction pattern indicate the presence of a physical interaction between the GO sheets and the rPET polymer matrix. A decrease of up to 10° in the water contact angle at 0.5 wt % GO loading; beyond this, it starts to increase due to the agglomeration of GO sheets. From this study, it is preferable to maintain the GO content to a maximum of 0.5 wt % to maximize hydrophilicity. This has the implication of enhanced filtration permeation flux in applications where hydrophilic membranes are desired.

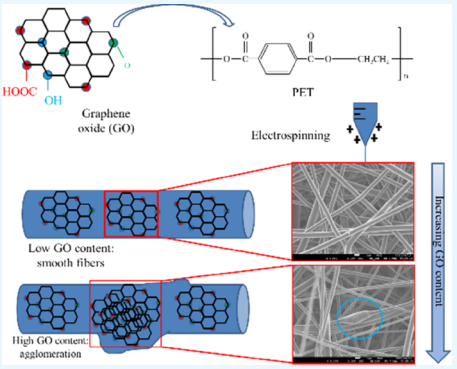

1. INTRODUCTION

Membrane-based technology, particularly polymer-based membranes, has gained a lot of attention in various applications such as filtration, energy cells, photocatalysis, sensing, etc.[1] In recent years, the highly porous nanofiber membranes, due to their ease of preparation and higher mechanical strength, have since replaced the various polymeric membranes prepared by the phase inversion method in gas and water separation for a more economical membrane separation.[2] Nanofibers have been used as porous substrates to support the dense and delicate thin film barrier layers used in ionic separation processes. Electrospun nanofiber membranes with their unique properties such as high surface area of the individual fibers, high porosity, and interconnected pores are highly permeable. They can thus increase the overall membrane performance.[1,3−5]

Electrospinning has become one of the most efficient and cost-effective nanofiber processing techniques, especially when it comes to the use of recycled material. Due to the growing concern over environmental issues triggered by polymer waste, the recycling of polymers such as poly(ethylene terephthalate) (PET) has attracted interest in the plastic industry. For example, postconsumer PET bottles are converted into highly valuable inexpensive fiber products compared to virgin PET. PET is a semicrystalline thermoplastic of the polyester family with a unique molecular structure and good chemical, thermal, and mechanical resistance. It is one of the commonly used thermoplastic polyesters in industrial applications such as food packaging and textile fibers due to the superior chemical, physical, and barrier properties; good processability; low cost; and recyclability.[6,7] The PET recycling process includes chemical or mechanical processing, whereby PET undergoes degradation. The degradation leads to a reduction in the polymer molecular weight and viscosity, thus leading to property deterioration, e.g., mechanical strength. To alleviate the shortcomings, rPET has been reinforced by blending with chain extenders, polymers, and cross-linkers. The incorporation of nanofillers such as silica (SiO_2), carbon nanotubes (CNTs), and graphene-based nanomaterials into the matrix[6,8,9] is the more preferred approach for filtration membranes as they maintain the permeability of membranes. Graphene-based

Received: May 17, 2021
Accepted: July 21, 2021
Published: August 4, 2021

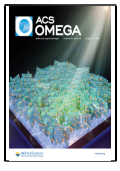

nanofillers such as graphene oxide (GO) are highly suited for membrane-based separation due to atomic thickness, high mechanical strength, and chemical inertness. GO is a renowned carbon-based nanomaterial, an intermediate graphene material with a novel nanostructure, and a precursor for reduced GO synthesis. GO is produced by the chemical exfoliation of graphite through the Hummers' method that involves the oxidation of low-cost graphite powder using a strong oxidizing agent such as $KMnO_4$ in the presence of a strong acid.[10] GO is a unique hydrophilic material with oxygen groups (O−H, −COOH, or C══O, −O−, i.e., epoxy, carboxyl, or hydroxyl). These negatively charged hydrophilic oxygen-containing functional groups offer better dispersibility in water and polar solvents due to improved hydration, exfoliation, and interaction with the functional groups of various polymer matrices. The use of nanomaterials within the polymer membrane layer is, therefore, one of the strategies that focus on improving membrane permeability.[1,3−5]

Graphene has successfully been incorporated into PET due to the possible chemical interactions of the oxygen functional groups with the aromatic groups of the polymer matrix, as shown by a quite significant enhancement in (mechanical) properties.[11] However, to our knowledge, no study has looked into the possible interfacial interaction and the effect of graphene/GO loading on the performance of recycled PET (rPET) nanofiber membranes. The GO content in electrospinning polymer solution affects the dispersion of the GO sheets as well as properties such as rheology, solution viscosity, and fiber diameter. The dispersion of graphene-based materials is the most important factor in the fabrication and performance of graphene-based polymer nanocomposites, particularly for gas and water transport in membranes. In combination with GO−polymer interaction, the dispersion of GO within the polymer matrix affects the performance of GO composite membranes. Fortunately, in electrospinning, the applied electrostatic stretching elongation forces on the GO−polymer solution are believed to overcome agglomeration while aligning and distributing the nanosheets evenly within the fibers. The well-dispersed and evenly distributed GO nanosheets within the nanofibers enable the fabrication of highly functional nanofiber composite membranes.[12−14]

Herein, the effects of GO loading on the properties of electrospun rPET are investigated. The solution properties were measured and correlated with the electrospinnability of the rPET/GO solution and the resulting fiber properties. The surface properties, including surface morphology and wettability, and the mechanical properties of the electrospun rPET/GO composites were investigated. Nanofiber membranes produced from the recycled polymer material combined with multifunctional fillers can thus be used in advanced applications such as gas sensors, biomedical devices, and capacitors.

2. RESULTS AND DISCUSSION

2.1. Morphology. The electrospinning of defect-free fibers is dependent on the polymer molecular weight and polymer solution concentration. Smooth bead-free fibers were obtained only when the rPET concentration was over 25 wt % to produce bead-free fibers. At this optimized concentration of rPET, the polymer solution possesses a stretchable rPET chain network that inhibits network rupture during electrospinning.[15] Electrospinning polymer solution with GO addition was prepared in a way that favors a homogeneous colloidal rPET polymer solution of dispersed GO nanosheets to avoid aggregation as much as possible. The GO was synthesized using the improved Hummers' method as described in the synthesis section. The synthesized GO was sonicated to obtain dispersed nanosheets. The distribution of GO nanosheets within nanofibers may differ from that of polymer films due to the confined space within the 1D nanofibers. In this regard, the distribution and location of the nanosheets are also affected by the compatibility between the rPET polymer solution and GO (e.g., solvent properties such as vapor pressure). In addition, the high surface area of graphene nanosheets has shown strong interactions with polymer matrices such as polystyrene (PS) and PET.[16,17] The presence of the oxygen-containing functional groups is expected to form hydrogen bonds with the polymer. Therefore, GO gives a better dispersion than the graphene counterpart with the $\pi-\pi$ conjugate effect that gives an uneven dispersion. Sonication also aids in the dispersion of the sheets in a polymer solution.[13,16]

Figure 1 shows the surface morphology and the diameter of the fabricated nanofibers examined by the scanning electron

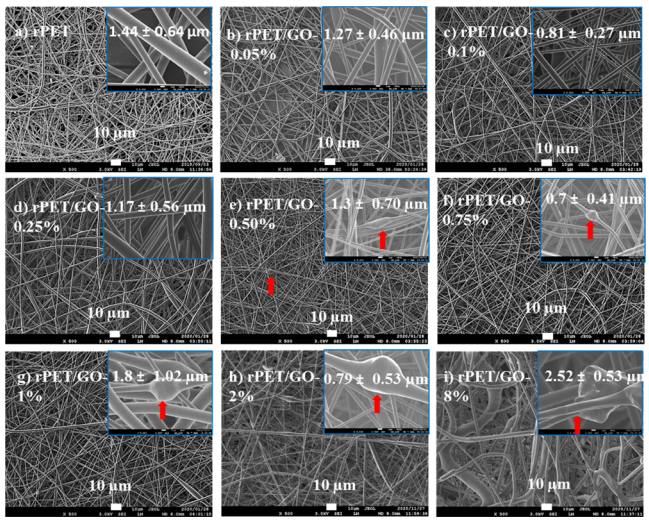

Figure 1. Scanning electron microscopy images of (a) rPET and (b−i) rPET/GO fiber membranes with various GO loadings. The insert of each image shows higher magnification images with the mean diameters.

microscope (SEM) images. The transmission electron microscopy (TEM) image of rPET fibers and the scanning TEM (STEM) image of rPET/GO composite fibers containing 0.75 wt % GO are reported in Figure 2. The smooth surface morphology was observed for rPET with node-like lumps starting to appear (as shown by the red arrows, Figure 1) for GO filled fibers, especially for the GO content of above 0.5 wt %. The STEM observation of rPET/GO composite fibers containing 0.75 wt % GO supports this observation. These bead-like or lumpy fiber surfaces are due to the agglomerated GO sheets, leading to a broader fiber diameter distribution. Again, this may be due to the poor GO distribution within the fiber strands during the electrospinning process. The diameter of the nanofibers initially decreased after the incorporation of GO nanosheets, from 1.44 μm for neat rPET to 0.77 μm for 0.75 wt % GO loading and 0.53 μm for 2 wt % GO loading. Thicker fibers than those of neat rPET were observed for 1 and 8 wt % loadings. However, with the viscosity values reported in Table 1, the diameter should

https://doi.org/10.1021/acsomega.1c02578
ACS Omega 2021, 6, 21005−21015

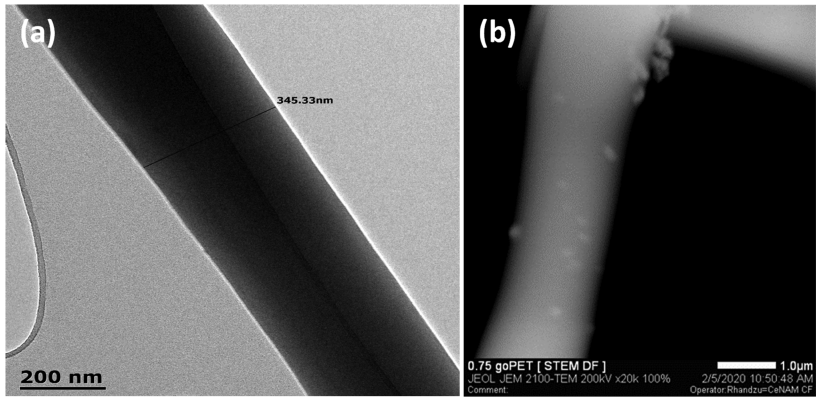

Figure 2. (a) Transmission electron microscopic image of the rPET fiber and (b) scanning transmission electron microscopic image of the rPET/GO composite fiber containing 0.75 wt % GO.

Table 1. The Viscosity of Various Solutions[a]

sample	viscosity (cP)	fiber diameter (μm)
PET	280	0.52 ± 0.11
rPET	180	1.44 ± 0.64
rPET/GO-0.1	180	0.81 ± 0.27
rPET/GO-0.25	240	1.17 ± 0.56
rPET/GO-0.50	260	1.30 ± 0.7
rPET/GO-0.75	180	0.77 ± 0.41
rPET/GO-1	180	1.81 ± 1.02
rPET/GO-2	160	0.59 ± 0.53
rPET/GO-8	240	2.52 ± 0.53

[a]The solution viscosity of various samples was measured using a Brookfield DV-I Prime digital viscometer, Brookfield Engineering Laboratories, Middleboro, MA, USA, spindle #6, at 25 °C.

increase with GO content due to the viscosity increase by the hydrogen bond interactions that reduced the stretching of the polymer solution during electrospinning.[11] As the highly volatile solvents like trifluoroacetic acid (TFA) are suitable solvents for polymers such as PET and poly(trimethylene terephthalate) (PTT), the presence of nodes or lumps could mean that there could be a phase separation between the polymer solution and the heavy GO sheets. The fast evaporation of the highly volatile solvents thus results in aggregation. This could also be due to the fact that the lateral dimensions of the GO sheets are larger than the fiber diameters.[15,18,19] Huang et al.[15] observed agglomeration due to phase separation when the GO loading reached 0.5 wt %, with a fiber diameter increase observed at 3 wt % GO loading.[15] GO is known to have residual sp^2 bonded carbon (graphene-like) capable of forming $\pi-\pi$ interactions with the aromatic rings of polymers such as PET.

Additionally, the hydrophilic groups (oxidized functional groups) stabilize the GO sheets with polar solvents and polymer matrices.[14] The aggregation was also observed for the electrospinning of polyesters such as PTT nanofibers incorporated with high GO loading (1−7 wt %) and highly volatile TFA.[15] Fibers at lower GO loadings of less than 0.5 wt % do not show any visible GO lumps and may thus represent the compatibility of the phases without phase separation or simply less aggregation.

The viscosity of PET reduces upon recycling, as observed in Table 1, as the viscosity of rPET is only 180 cP compared to that of unrecycled or virgin PET (280 cP). The reduction in viscosity is due to the reduction in the molecular weight through chain scission during the recycling process. On the other hand, the viscosity was enhanced upon the addition of GO nanosheets at a loading of 0.25 and 0.5 wt % due to the strengthened hydrogen bonding interactions induced between GO and the polymer matrix.[13] Park et al.[13] also observed a fiber diameter increase with GO loading (0.1−1.05 wt %) due to the increase in viscosity by the intermolecular hydrogen bonding interactions, thus reducing stretching during electrospinning and producing thicker fibers.[11] The decrease in fiber diameter, despite the high solution viscosity (at 0.25 and 0.50 wt % GO loadings), indicates that the GO (i.e., electrical conductivity) can dominate fiber diameter reduction than viscosity. At higher GO loadings >0.50 wt %, however, the solution viscosity plays a role as observed by low viscosity values. At GO loadings higher than 0.50 wt %, aggregation caused by the restacking of GO sheets diminishes the GO sheets' nanofiller effect.

The amount of GO content affects the dispersion and polymer solution rheological properties, thus indirectly affecting the resulting fiber diameters.[20] Viscoelastic measurements were conducted to understand the effect of GO nanosheets on the 25% rPET polymer solution. Figure 3a shows that the solutions exhibit a Newtonian behavior. This is typical of PET polymer solutions,[21] with rPET having a lower viscosity than PET. Figure 3b shows the rheological properties of the PET/rPET, i.e., (b) storage modulus (G') and (c) loss modulus (G'') versus frequency curves of PET and rPET. The results show that G' is higher for the PET than the rPET polymer and the difference became far greater at higher frequencies, while G'' increases linearly for both polymers for the duration of the test. Due to their large surface area, among other properties, the inclusion of nanoparticles also gave rise to changes in solution properties such as the rheological behavior due to attractive or repulsive forces between the polymer and nanoparticles (GO sheets).[22] Figure 3a shows the viscosity (η) vs shear rate for rPET/GO solutions at varying GO loadings. First, it is clear that the η of PET is reduced after recycling (rPET) due to the loss in molecular weight by thermal degradation. The viscosity data displayed in Table 1 show that the reduction in viscosity was from 280 cP for PET to 180 cP for rPET. Secondly, the η of rPET is reduced after GO addition (except for the 0.75% GO content); this is consistent with reducing elongation at break for the GO composite membranes. This observation of η reduction has been related to the increase in the free volume at the GO sheets of large surface area and rPET polymer chains, increasing the

https://doi.org/10.1021/acsomega.1c02578
ACS Omega 2021, 6, 21005−21015

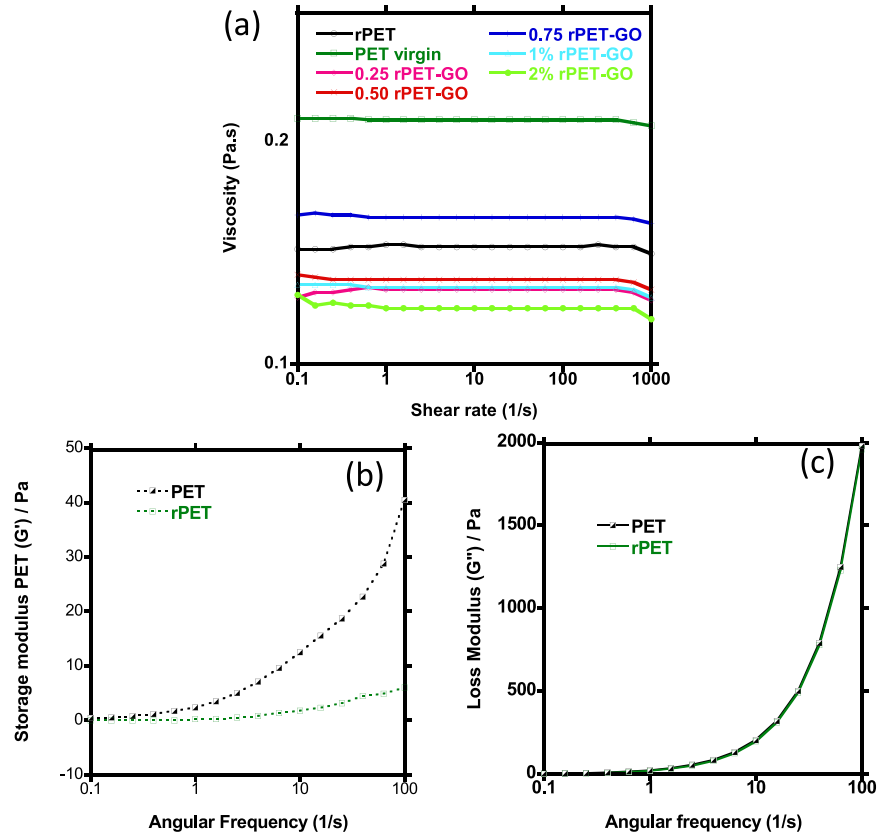

Figure 3. (a) Shear viscosity (η^*) of rPET solutions at various GO loadings. The viscoelastic properties of the rPET solutions with various GO loadings at a temperature of 27 °C. Frequency dependence (b) storage (G') and (c) loss (G'') moduli of PET before and after recycling (rPET) at a temperature of 270 °C under a nitrogen environment.

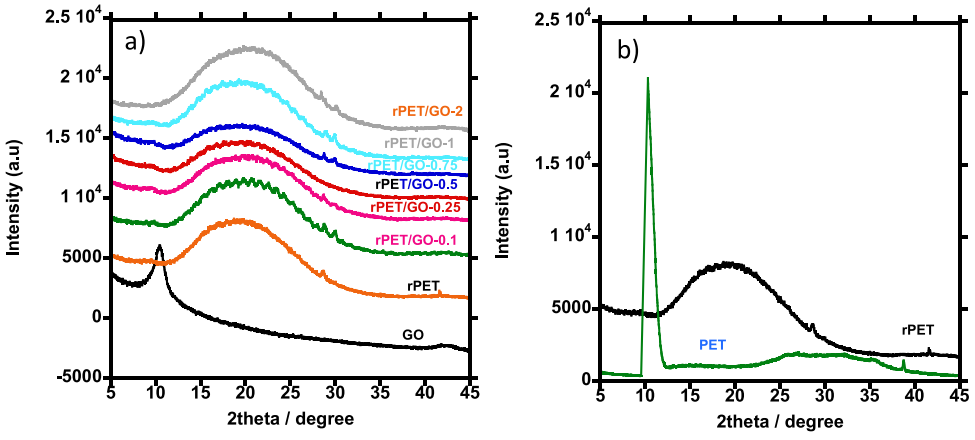

Figure 4. XRD patterns of the (a) GO powder, neat rPET, and rPET/GO composite membranes at various GO loadings and (b) neat PET and rPET.

interfacial area inside the rPET polymer solution and thereby reducing the solution viscosity.[18,23] When the viscosity increases, there is an enhancement of the macromolecular entanglement with GO addition indicating a stronger interaction at the polymer−GO interface.[22] The decrease in viscosity also leads to the reduction in fiber diameter with GO loading. Furthermore, the slight reduction in fiber diameter with GO addition can be attributed to the repulsive action between the hydrophilic GO sheets and hydrophobic rPET polymer chains. At higher GO loadings (>1%), possible GO agglomeration usually causes a substantial viscosity decrease at the interaction sites of GO with polymer chains. As the surface area of GO is decreased, the adsorbed polymer onto the GO sheets is almost totally covered by the agglomerated nanosheets. A small portion of polymer available in the solution leads to a decrease in viscosity. A decrease in polymer solution viscosity was also observed for the nonpolar PS and polar GO, while there was an increase in polymer solution viscosity with nanoparticle addition for the polar polymer such as PAN, due to polar−polar interaction between hydrophilic ZnO particles and polar PAN polymer solution.[22]

2.2. Structural Analysis Using X-ray Diffractometer. Figure 4 shows X-ray diffraction (XRD) patterns for the GO powder and electrospun rPET/GO composite membranes.

https://doi.org/10.1021/acsomega.1c02578
ACS Omega 2021, 6, 21005−21015

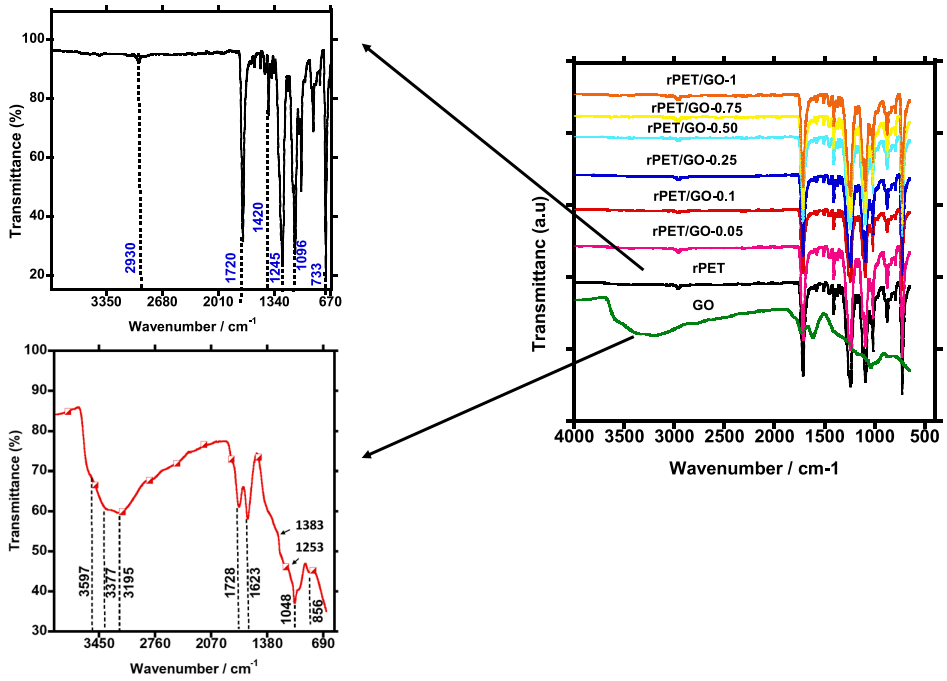

Figure 5. Fourier transform infrared spectra of (a) electrospun rPET−GO composites, (b) synthesized GO powder, and (c) neat rPET.

The GO powder was characterized by a prominent diffraction peak at 2θ of 9.7 and 42.2°, associated with the (002) and (100) crystal lattice, corresponding to a *d*-spacing of 0.884 and 0.214 nm. This is also an indication of the successful synthesis of GO without contaminants.[24,25] For rPET, a broad, amorphous halo was observed at 2θ = 21°, and this suggests that the electrospun rPET membrane possesses no crystalline phase, thus showing the amorphous nature of rPET. Although PET is a semicrystalline polymer, the lack of crystallinity in electrospun fibers is attributed to the rapid solidification of polymer jet during the electrospinning process.[8] The broad peak remains broadened upon the addition of GO until 1 wt %, where it starts to narrow slightly. The XRD patterns of the rPET/GO composite at various GO contents show the diffraction peaks similar to those of the rPET structure while not showing any characteristic peak of GO sheets. This may be attributed to the homogeneous dispersion and high degree of GO distribution within the rPET matrix.[26] In addition, the rPET chains completely covered the graphene sheets. Similar trends have been observed in literature for well-dispersed and fully exfoliated GO sheets within polymer matrices.[27] For example, PET polymer films prepared by extrusion showed more dispersed GO sheets that offered more exposure of the GO sheet surface within the polymer matrix.[7] The interactions in the interface between GO and the polymer matrix were thus improved. This also means that there were no significant changes in the *d*-spacing of the rPET/GO composites for all the GO loadings, homogeneously dispersed and separated by the polymer phase, with fewer multilayered sheets in the matrix.[24] On the contrary, the presence of characteristic GO peaks in the GO−polymer composite membranes has also been seen as an indication of the dispersion of GO along the membrane surface to show the GO migration toward the membrane surface for other membrane processing methods such as phase inversion.[27]

2.3. Chemical Structure by Fourier Transform Infrared (FTIR) Spectroscopy. The FTIR spectra of the synthesized GO powder, neat rPET, and rPET/GO electrospun composite fibers at various GO loadings are shown in Figure 5a−c. The FTIR spectra of the GO powder with the various oxygen-containing functional groups are detected at 3377 cm^{-1} (hydroxyl O−H for free H_2O molecules), ∼1728 cm^{-1} (C═O for the carboxylic group), and ∼1623 cm^{-1} (C═C stretching for the GO sp^2). In addition, at ∼1383 cm^{-1} (O−H bending for bound H_2O molecules), ∼1253 cm^{-1} (C−O for the epoxy-functional group), and ∼1048 cm^{-1} (C−O−C for the alkoxy group vibrations),[19,28,29] as shown in Figure 5a,b. The broad IR band between 2800 and 3600 cm^{-1} is attributed to the stretching of the O−H functional groups (i.e., water adsorbed within the GO layers). The stretching at 3597, 3377, and 3195 cm^{-1} indicates three types of O−H groups (alcohol, phenol, and COOH).[27] rPET peaks are related to the intrinsic structure of PET (Figure 5a,c). The band at 1720 cm^{-1} was the terephthalic acid ester −C══O group, a degradation byroduct that may have formed during the recycling of PET. The peak at 1420 cm^{-1} is for the deformation of carboxylic acid due to terephthalic acid. The small peak at 2930 cm^{-1} is the C−H axial of the aromatic structure found in the polymer. C−C−O and the O−C−C stretching at 1245 and 1096 cm^{-1}, respectively. The C−H vibration at 733 cm^{-1} is also for the aromatic structures.[30] FTIR can also be used to determine the effect of GO on the crystallinity of the polymer. However, in our case, there was no change in the chemical structure of rPET after the incorporation of GO, as there was no chemical interaction between the filler and matrix.

In Figure 5a, there is no shift or additional shoulder peaks in the rPET characteristic peaks; i.e., the hydroxyl groups in rPET did not shift to a lower wave number to indicate hybridization of rPET with GO, similar to the PVA-GO nanofibers as observed by Park et al.[13] Others observed characteristic GO peaks in the polymer matrices of their polymer−GO systems due to the chemical interaction between the hydrogen donating groups in GO and polymer functional groups such as the carbonyl groups of poly(ε-caprolactone). The visible

https://doi.org/10.1021/acsomega.1c02578
ACS Omega 2021, 6, 21005−21015

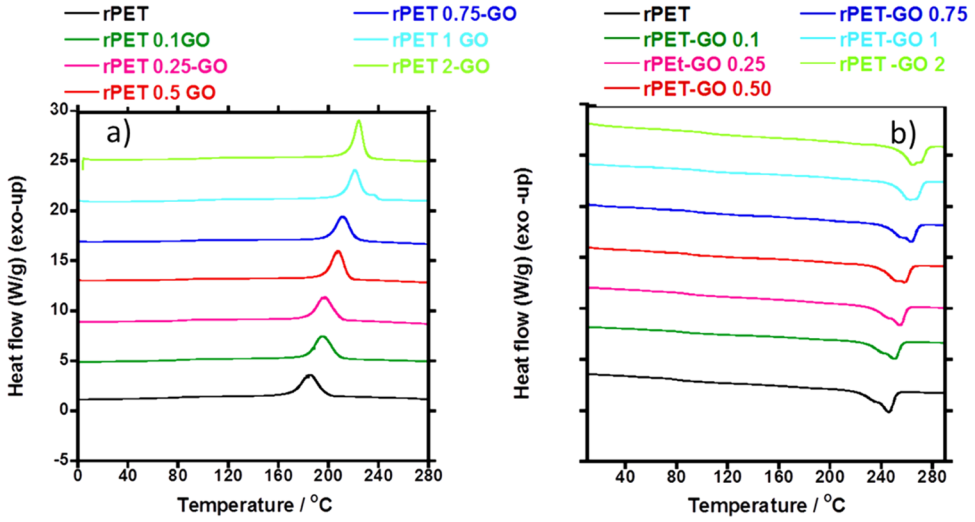

Figure 6. Differential scanning calorimetric thermograms of rPET and various rPET/GO fiber samples. (a) Cooling curves and (b) the corresponding heating curves. Samples weighing approximately 5 mg first underwent cooling to −20 °C and then were heated to 290 °C under a nitrogen atmosphere (at a flow rate of 25 mL min^{-1}).

Table 2. DSC Data Obtained from the Second Heating and Cooling for rPET/GO Membranes at Various GO Loadings[a]

sample	T_m (°C)	T_g (°C)	ΔH_m (J/g)	X_c (%)	T_c (°C)	ΔH_c (Jg^{-1})
rPET	246.2 ± 0.22	75.3 ± 0.85	41.84 ± 0.18	29.89	184.8 ± 0.60	41.63 ± 0.06
rPET/GO-0.1	246.6 ± 0.03	75.0 ± 1.02	43.47 ± 1.41	31.34	190.1 ± 1.53	43.86 ± 1.67
rPET/GO-0.25	246.7 ± 0.12	79.85 ± 0.49	40.37 ± 0.36	28.90	189.1 ± 0.06	42.40 ± 2.51
rPET/GO-0.5	246.4 ± 0.29	73.70 ± 0.11	43.44 ± 0.47	31.18	196.1 ± 1.10	42.91 ± 0.65
rPET/GO-0.75	247.5 ± 0.19	73.97 ± 1.64	44.53 ± 3.51	34.86	196.0 ± 1.40	46.32 ± 2.78
rPET/GO-1	241.8 ± 1.24	72.70 ± 0.11	45.39 ± 0.47	33.87	200.9 ± 0.36	46.96 ± 1.01
rPET/GO-2	240.8 ± 0.13	75.2 ± 0.35	43.88 ± 4.29	32.61	200 ± 0.49	44.74 ± 3.53

[a] T_m, melting temperature; T_g, glass transition temperature; T_c, crystallization peak temperature; ΔH_m, enthalpy of melting; ΔH_c, enthalpy of crystallization; and X_c, degree of crystallinity.

GO peaks within the host polymer thus indicate a homogeneous dispersion and strong interactions between GO and the host polymers.[7,28]

2.4. Thermal Properties. The thermal properties of rPET/GO fibers were studied, and the DSC results are shown in Figure 6. Figure 6a shows the cooling thermograms of GO filled rPET fibers from 290 to −20 °C, while Figure 6b shows the corresponding second heating curve from −20 to 290 °C. The crystallization behavior of rPET and rPET/GO composite membranes, the crystallization temperatures (T_c) and crystallization enthalpies (ΔH_c), and various other calculated parameters are summarized in Table 2. From part (a) of Figure 6, we observe the nucleation of crystallization of rPET by GO. The higher the content of GO was, the more pronounced was the nucleation. The T_c value increased from 184 °C for the neat PET, 196 °C for the 0.5 wt % content, and 200 °C for the rPET with 2 wt % GO. Apart from the 0.25 wt % loading, T_c increases with an increase in GO loading. This shows that higher T_c values translate to a stronger interfacial interaction of the sheets with the polymer.[29] The amorphous rPET showed some degree of crystallinity (X_c) due to a high degree of molecular orientation within fibers induced during electrospinning. The X_c values for rPET/GO showed no significant changes. The decrease in X_c and the increase in T_g in other studies suggest some extent of interaction between the polymer and GO nanosheet filler.[14] The change in X_c also indicates a change in chain mobility.[14,23] ΔH_c increased slightly with GO loading. A slight increase in crystallinity is unlikely to translate to higher mechanical properties, as will be shown later.

The second heating curves in Figure 6b show that the rPET−GO membranes undergo a melting transition with the endothermic peaks (T_m) of rPET at around 246 °C. The inclusion of GO within the PET nanofibers did not significantly affect T_m and T_g values. Slight T_m changes were observed at 1 and 2 wt % loadings with a reduction from 246 to 240 °C. The T_g was unchanged at 75 °C, and a slight change was observed for 0.25 wt % loading. The slight increase in T_g for 0.25 wt % loading is also associated with a slight decrease in crystallinity X_c and T_c. This may be due to a better interaction among all the other rPET/GO samples, as indicated by the higher modulus in the next section. A melting peak with a shoulder appearing is also observed for the neat rPET as well as rPET/GO composites. Other studies have shown negligible T_m and ΔH changes at low GO loadings and only started observing the changes at higher loadings above 2 wt % for casted film samples. An increase in T_g with GO content usually explains the effective interaction between the polymer and nanosheets.[31] Other studies have shown that the addition of GO enhances the X_c of melt mixed PLA/PCL composites.[29] Others indicated T_c shifting to a lower temperature, while the T_m and T_g remained unchanged for the electrospun PTT nanofibers with thermally reduced GO.[15] However, in other studies, the T_g for both PVA nanofibers and film composites seems to be enhanced by GO loadings. The enhancement at high loadings of 3−7 wt % or low loadings of 0.1−0.5 wt % was

https://doi.org/10.1021/acsomega.1c02578
ACS Omega 2021, 6, 21005−21015

Table 3. Mechanical Properties of the GO Filled rPET Membranes

sample	fiber diameter (μm)	modulus (MPa)	tensile strength (MPa)	elongation at break (%)
PET	0.52 ± 0.11	456 ± 44.6	26.5 ± 1.43	282 ± 13.0
rPET	1.44 ± 0.64	368 ± 34.2	29.48 ± 2.3	334 ± 38.0
rPET/GO-0.1	0.81 ± 0.27	302 ± 19.6	13.6 ± 0.8	218 ± 20.0
rPET/GO-0.25	1.17 ± 0.56	362 ± 25.5	13.6 ± 0.6	213 ± 8.8
rPET/GO-0.50	1.3 ± 0.7	191 ± 30.0	13.3 ± 1.4	201.5 ± 15.4
rPET/GO-0.75	0.77 ± 0.41	322 ± 14.6	15.3 ± 1.0	201.6 ± 19.8
rPET/GO-1	1.81 ± 1.02	284 ± 28.0	12.4 ± 0.8	224.6 ± 15.8
rPET/GO-2	0.59 ± 0.53	320.7 ± 27.6	13.63 ± 0.96	193 ± 9.9
rPET/GO-8	2.52 ± 0.53	351 ± 35.3	8.01 ± 0.66	44.53 ± 2.4

attributed to the good interaction between fully exfoliated GO sheets and hydrophilic PVA polymer matrices due to restricted chain movement caused by the GO sheets.[13,15,31] The T_g has shown an indication of the state of chain mobility, which increases by the effective interaction between the nanofiller and polymer due to hydrogen bonding between GO nanosheets and polymers (e.g., PVA polymer films with GO loading 0.5−3.5 wt %).[28,31]

2.5. Tensile Properties. The tensile properties of electrospun rPET−GO membranes are summarized in Table 3. The rPET obviously exhibits a lower tensile stress than the original PET due to much thinner fibers of PET (0.52 μm) compared to the recycled PET fibers (1.44 μm), as deduced from the decrease in the viscosity of rPET as compared to that of pristine PET. During recycling, PET comes into contact with contaminates (such as PET bottle labels and caps) and some degree of thermal degradation during reprocessing (remelting by extrusion). These conditions cause a reduction in the intrinsic viscosity of PET.[32] As shown by the viscosity measurements shown in Table 1, the viscosity of rPET was 180 cP, while that of virgin PET is 280 cP, while the M_w of 382 kg/mol was reduced to 73 kg/mol for rPET (as per rheology M_w analysis). The addition of 0.1% GO did not have any changes in rPET viscosity. The GO loading of 0.25 and 8 wt % increased the viscosity to 240 and 260 cP, combined with an increase in diameter and modulus. The exception is the 0.5 wt % loading displaying the lowest modulus. The tensile results show that, upon the addition of GO to the rPET, the modulus and elongation at break decreased for all GO loadings. At the same time, the fiber diameters also decreased and then increased for the 8 wt % loadings. A decrease in fiber diameter with GO content for nanofibers is a common trend, decreasing viscosity, as previous studies have shown a decrease in fiber diameter with GO addition.[13] However, in the current study, the fiber diameter decreased while viscosity also increased with GO content (except for 0.75, 1, and 2 wt % with low viscosity), although the opposite was observed with the shear viscosity measurements shown in Figures 1 and 2. The same was observed in a study by Huang et al.[15] They also observed a fiber diameter decrease with GO loading of 1 wt % and then an increase at higher GO loadings of 5 and 7 wt % for PTT/graphene fibers, as we observed with the 8 wt % loading with the 2.52 μm diameter.[15] The initial fiber diameter reduction, regardless of the viscosity increase, was due to an increase in conductivity caused by the presence of GO (as a graphene-based material).[15] Ramazani and Karimi[18] also observed an increase in conductivity in their PCL/GO polymer solution because of the sp^2 and sp^3 carbon domains in the GO responsible for electron transportation. This increases the polymer jet stretching due to an increase in electrostatic stretching, which explains the fiber diameter reduction upon GO addition.[18] Conducting polymer solutions with more conductivity lengthen the duration of charge dissipation during electrospinning, thus leading to fiber thinning.[13,33] Generally, for fiber membranes without nanofiller (GO) addition, thinner fibers are a result of a decrease in solution viscosity and generally lead to an increase in modulus and tensile stress (due to increased polymer jet stretching during electrospinning, thus leading to a higher degree of polymer chain alignment).[8] A similar observation of the reduction in tensile properties at low GO loadings of 0.05 to 0.25 wt % was also made for compression-molded films for polymer blends such as PLA/PCL, whereby the decrease in modulus is attributed to the ease in penetration of the thin GO sheets within the polymer, leading to the formation of nanovoids within the polymer matrix upon the addition of GO sheets. The unsonicated GO sheets could also be the reason for the susceptibility to agglomeration,[23] whereas sonication was conducted in the current study. It is worth noting that voids can be an indication of poor interconnection between GO and the polymer, thus leading to the creation of weakness points for the films during tensile testing.[24] The results in Table 3 also show that the elongation at break for the rPET/GO composites shows a decrease of between 30 and 39% compared to the neat rPET. The elongation at break decreases with GO loading mainly because an increase in GO content leads to brittleness in the membranes.[23] Lee et al.[19] also observed little or no effect of GO on mechanical properties for PAN/GO nanofibers at low GO loadings of 0.1 to 0.4 wt %.[19] Enhancement in mechanical properties (modulus and strain) were obtained for higher GO loading was observed at higher GO loadings of 2 wt % and higher as reported by Shin et al.[27] for GO loaded hydrogel films. Enhancement in mechanical properties is usually associated with a homogeneous dispersion of nanofillers within polymers. In most cases, this can be achieved by the method of exfoliation (e.g., thermal) or sonication level.[27] However, for nanofiber composites, higher GO concentrations (for example, >0.4 wt %) lead to GO agglomeration, phase separation, and irregular fiber diameter.[19] Interestingly enough, a decrease in modulus and tensile strength as well as an increase in the elongation at break was observed for thermally reduced GO in PTT polymer nanofibers at higher GO loadings of >1 wt %, which was said to be due to the misalignment of sheets during the electrospinning process. Therefore, it can be quite usual to observe a mechanical reduction in nanofibers due to the unstable alignment of rPET chains during the electrospinning of the rPET/GO solution; as the polymer solution viscosity increased upon the addition of GO content >0.25 wt %, the fiber diameter decreased slightly and then increased at higher GO loadings of 1 and 8 wt %. Ghasemi et al.[28] reported a

https://doi.org/10.1021/acsomega.1c02578
ACS Omega 2021, 6, 21005−21015

partial agglomeration of GO sheets at GO loading >0.05 wt %, which resulted in instability in the electrospinning jet and thus nonuniform fiber diameters.[28]

In summary, the reduction in polymer−GO modulus and tensile strength is ascribed to the poor dispersion and agglomeration of the GO particles for both low and high GO loadings, both for polymer films and for nanofiber composites.[15,23] The increase in modulus and tensile strength of fibers at low GO loadings is usually achieved by electrospinning polymer solutions with uniformly dispersed individualized GO.[34] The degree of exfoliation mostly depends on the GO synthesis method and to the extent or level of exfoliation; e.g., fully exfoliated sheets have less number of GO sheets stacked together. Therefore, the synthesized GO sheets in the current study may have not fully and individually exfoliated. Additionally, the dispersion of GO within nanofibers also depends on the polymer chemical structure and the solvent properties. Dispersion of GO nanosheets in the PET solution was also assisted with the interactions of oxygen functional groups (epoxy, hydroxyl, carboxyl, and carbonyl as confirmed by the FTIR spectra) with polar groups of PET as well as the weak $\pi-\pi$ interaction of the GO basal plane with a styrene ring of PET.[34,35]

The degrees of dispersion, orientation, and interfacial adhesion are the key factors affecting the end properties of polymer nanocomposites. GO nanosheets are expected to align in the direction of elongation during the stretching of a jet during electrospinning. The applied voltage creates a high electrical field, which can improve the nanofiller−polymer matrix interactions, thus improving the filler/matrix coupling at the interface at a molecular level (microstructure) as the dispersion is determined by the interfacial interaction as well as adhesion strength and reinforcement efficiency. In addition, the reinforcement ability of GO is correlated to intrinsic properties of GO nanosheets, the dispersion state of GO within a polymer matrix, and changes in crystallinity of semicrystalline polymers.[28]

With that being said, the reason for alignment is good homogeneity and interface strength, and when well dispersed, they form a highly oriented microstructure (become highly oriented) and co-continuous network within the polymer matrix, which will then lead to an enhancement in polymer performance such as mechanical, electrical, and thermal. This has been observed more especially for polymer composites prepared by melt processing. Thus, the dispersion of GO within the polymer matrix influences the properties of composites. A good dispersion at a molecular scale is achieved when there is a nanofiller−polymer matrix interaction through chemical bonding or intermolecular interaction (through the oxygen-containing functional groups of GO) between the nanofiller and polymer matrix. GO has been introduced into the polymer matrix of polymers such as PVA.[26]

2.6. Surface Wettability by Water Contact Angle (WCA) Measurements. Membrane wettability plays an important role in aiding in the permeability of water filtration membranes. Since PET is a hydrophobic polymer, hydrophilic GO with oxygenated functional groups was expected to enhance the membrane's wettability to contribute toward membrane permeability performance. The addition of GO into the rPET membranes resulted in a slight decrease in the water contact angle. Figure 7 shows a decreasing trend in WCA with GO loading up to 0.5 wt %. The water contact angle for PET nanofibers has been reduced by 10° (i.e., from 129 to 119°) by

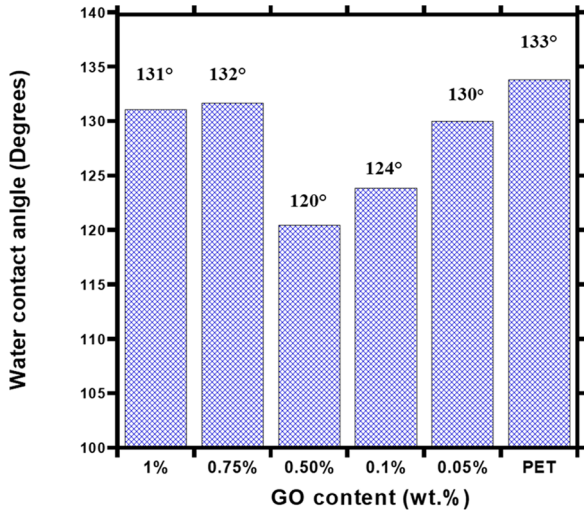

Figure 7. Water contact angles for rPET and rPET/GO composite membranes.

the addition of 0.05 wt % GO;[34] a similar reduction was obtained with the addition of 0.1 wt % in the current study, from 133 to 124°.

Moreover, the addition of 0.05 wt % GO had the WCA reduced by only 3° from 133 to 130°. With a similar preparation procedure, a slight decrease in WCA may be attributed to the fact that GO is embedded within the rPET matrix, exposing only a small amount of GO on the nanofiber membrane surface. As the GO content increases to 0.75 wt %, the WCA increases as it becomes more hydrophobic; this may be due to the poor dispersion of the agglomerated GO sheets, as indicated by the previous SEM images in Figure 1. Lai et al.[36] observed significant differences in WCA after GO addition for membranes prepared by phase inversion (i.e., a 13% increase).

In contrast, no changes were observed for the top coating layer membrane prepared by interfacial polymerization, probably due to the highly hydrophilic nature.[35] The effectiveness of GO loading is therefore also affected by the processing method.[36] For electrospun GO−nanofiber composites, another way of exposing the GO nanosheets onto the surface is by core−shell electrospinning by having a GO solution (a dilute rPET/GO solution) as a shell.[34] Therefore, for the electrospinning method, GO loadings of less than 0.5 wt % seem to favor a reduction in WCA, as loadings higher than 0.75 wt % increase the WCA as fewer GO sheets are available on the fiber surface due to aggregation.

3. CONCLUSIONS

The study reports the effect of GO loading on the solution, microstructure, and mechanical properties of rPET/GO composite fibers. The fiber morphology, mechanical properties, and wettability were investigated based on the dispersion and interfacial property of the GO nanosheets within the rPET polymer matrix. The smooth nanofiber surfaces at GO loadings lower than 0.5 wt % show that the nanosheets were well dispersed and highly intact within the rPET polymer matrix. For loadings above 0.5 wt %, lumps on fiber surfaces were observed due to the GO agglomerates. In addition, the fiber diameter decreased with GO loading. However, for high loadings of 1 and 8 wt %, the fiber diameters were higher than those of neat rPET. Despite the tendency of viscosity increase

https://doi.org/10.1021/acsomega.1c02578
ACS Omega 2021, 6, 21005−21015

with GO loading, the fiber diameter decrease may be attributed to the conductivity of GO or the repulsion between hydrophilic GO sheets and hydrophobic rPET polymer chains as indicated by the decrease in shear viscosities. However, the reduction in tensile strength, modulus, and elongation at break decreased with GO loading compared to neat rPET. This may be due to a possible misalignment in GO sheets within the fiber matrix. The 0.25 and 8 wt % GO loadings show a better performance in GO loaded fibers in terms of modulus, which can be associated with the high viscosity and thicker fibers. No chemical interaction was revealed by FTIR analysis as there were no characteristic GO peaks observed within the rPET polymer matrix for all GO loadings. This indicates that the chemical structure was not affected by GO incorporation and homogeneous dispersion of GO within rPET polymer at low loadings. For thermal analysis, the T_c gradually shifts to a higher temperature with GO loading to indicate the nucleating effect of GO. An increase in T_c with GO addition shows the strong interaction with the polymer. However, the unchanged T_m and T_g values after GO addition (with only a negligible T_m reduction at high GO loadings) did not indicate any chemical interaction between the polymer matrix and GO filler, hence reduction in mechanical properties after GO incorporation, mainly due to the low level of GO sheet exfoliation. Hence, there was no consistent correlation between the mechanical properties and GO loading. A slight improvement in WCA was observed at GO loadings below 0.5 wt %. Therefore, based on the tensile properties and WCA, lower loadings favored a better dispersion of GO within the rPET polymer and were considered optimum for homogeneously dispersed GO. The dispersion at low loadings is based on the compatibility and physical interaction between GO and rPET due to the high surface area. Therefore, for the current study, the enhancement in performance of the rPET fiber membrane can still be achieved by achieving a higher exfoliation of the GO nanosheets prior to electrospinning.

4. EXPERIMENTAL SECTION

4.1. Materials and Methods. Recycled PET (rPET) pellets were obtained from Mpact Recycling, South Africa. The viscosity average molecular weight was 73.06 kg/mol. Trifluoroacetic acid (TFA), dichloromethane (DCM), phosphoric acid (H_3PO_4), hydrochloric acid (HCl), sulfuric acid (H_2SO_4), potassium permanganate ($KMnO_4$), and hydrogen peroxide (H_2O_2) were all purchased from Sigma Aldrich, South Africa. The density of the synthesized GO powder was 1.86 g/cm^3 as measured by a pycnometer (Micromeritics AccuPyc II 1340, USA).

4.2. Synthesis of GO. GO sheets were prepared by using the improved Hummer method according to Marcano et al.[10] It is the chemical oxidation of natural graphite powder, whereby the first step is the oxidation of graphite to produce graphite oxide, which is subsequently exfoliated in the solution to obtain GO. The typical procedure was as follows: A concentrated acid mixture of H_3PO_4 and H_2SO_4 (1:9, volume equivalent) was added to 3 g of graphite powder and stirred for 20 min at 25 °C. The small portions of $KMnO_4$ (6 wt % equivalents of graphite powder, i.e., 18 g) were added slowly to the above mixture. Later, the reaction mixture was heated at 50 °C with constant stirring for 14 h. Following the completion, the reaction mixture was cooled naturally and then poured on ∼500 mL of ice water with 5 mL of H_2O_2 (30%). To remove Mn impurities, the solution was further diluted with deionized water and centrifuged several times at 4000 rpm. The collected residue was again mixed with 200 mL of 30% HCl and centrifuged (4000 rpm) using ethanol (400 mL) and deionized water (1 L), and the supernatant was discarded away. The obtained dark-brownish product (graphite oxide) was redispersed in deionized water and ultrasonicated for 2 h to get GO sheets. Finally, the centrifuged product was dried in a vacuum oven at 60 °C to obtain a dried GO sample. The AFM (images are not reported here) was used to measure the lateral size and thickness of the synthesized GO, which were found to be 15.5 nm and 0.246 × 1.872 μm, respectively. Compared to fiber diameters, although in their clustered form, the sizes of the clusters were found to be as high as 3.08 μm. Therefore, with such large-sized agglomerates, the incorporated GO is expected to be visibly protruding along the fiber surface as clumps shown on the SEM and STEM images (Figures 1 and 2).

4.3. Preparation and Properties of rPET/GO Solutions. To prepare rPET nanofibrous membranes incorporated with varying GO contents via electrospinning, homogeneous rPET and rPET/GO solutions were prepared. The rPET solution of 25 wt/vol % was used to study the effect of GO loading on the rPET membranes. A series of GO dispersions were prepared by adding GO powder to DCM/TFA 3:7. Subsequently, sonication was performed for 1 h to disperse the GO sheets evenly within the polymer solution, which was previously prepared as follows: Weighed rPET pellets (2.5 g) were added to the TFA/DCM solvent mixture to make a 25 wt % polymer solution followed by stirring at 25 °C for 24 h to dissolve the rPET pellets. The GO content was varied at 0.05, 0.1, 0.25, 0.5, 0.75, 1, and 2 wt % loadings, which correspond to 99.9/0.1, 99.75/0.25, 99.5/0.50, 99.25/0.75, 99/1, 98/2, and 92/8 polymer to filler weight ratios, respectively. The volume fraction was obtained by using the densities of GO and rPET. The viscosities of the solutions were conducted by using a Brookfield DV-I Prime digital viscometer, Brookfield Engineering Laboratories, Middleboro, MA, USA, spindle #6, at 25 °C.

The viscoelastic properties of the rPET/GO solutions and melt rheological measurements (for M_w determination) of PET before and after recycling (rPET) were performed by using a Physica MCR501 rheometer (Anton Paar, Austria) at a temperature of 270 °C. The rheological properties were measured by using a 25 mm diameter parallel plate geometry under a nitrogen environment. Disc-shaped compression-molded samples with a thickness of about (1.68 mm) were measured with a strain amplitude of 5% and zero-gap of 1.15 mm. Oscillatory shear experiments were used to determine the storage modulus (G'), loss modulus (G''), and complex viscosity (η^*) of the rPET/GO solutions.

4.4. Electrospinning of rPET/GO Fiber Membranes. The prepared solutions were electrospun at 25 °C by using a commercially available apparatus from IME Technologies. The horizontal electrospinning setup consisted of a stainless steel drum collector 25 cm in diameter and rotating at 100 rpm and covered with aluminum foil for fiber collection, functioning as a ground or negative electrode. The polymer solution was pumped by using a standard IME Technologies syringe pump (Harvard Apparatus EP-H11) to accurately control the flow of the polymer solution from a 10 mL glass syringe fitted with a luer lock and connected via a capillary Teflon tube with 1 mm internal diameter to a blunt 1.0 × 0.8 mm 2 L gauge stainless steel needle, serving as a positive electrode. The prepared polymer solutions (rPET/GO) at varying GO loadings were

https://doi.org/10.1021/acsomega.1c02578
ACS Omega 2021, 6, 21005−21015

then electrospun at the following conditions: 15 kV, 15 cm spinning distance, and 5 μL/min flow rate, which were the previously optimized electrospinning parameters.

4.5. Characterization. The surface morphology of the fibers of the rPET/GO membranes was observed by using SEM (JEOL JSM-7500F, Tokyo, Japan) operated at an accelerating voltage of 3 kV and emission current of 10 μA under high vacuum (9.5×10^{-5} Torr). Prior to imaging, the fiber membrane samples were sectioned and coated with a carbon coater to render them conductive under the electron beam. The fiber diameters were determined using a commercially available image analysis program (Image J software, https://imagej.nih.gov/ij/). About 100 individual fibers were measured per sample to obtain the mean fiber diameter. Multimode atomic force microscopy (AFM, Nano Scope Version (R) IV, London, UK) was used to characterize the GO sheets' height, lateral size, and thickness. Droplets of GO suspensions were cast onto a silicon wafer substrate, air-dried, and mounted into an AFM stump before characterization. Transmission electron microscopy (TEM) was used to study the morphology of the rPET fiber and GO-containing rPET composite fiber. A small piece of nanofiber mat sample was cut and immersed in ethanol and sonicated to evaluate the morphology of fibers. Before sonication, the nanofibers were loosened with a tweezer to isolate each fiber strand from the nanofiber mat individually. Images were collected on a JEOL 2100F TEM instrument operated at 200 kV. Attenuated total reflectance (ATR) FTIR spectroscopy using a Perkin-Elmer Spectrum 100 spectrometer in the wavelength region of 800 to 4000 cm^{-1} was used with 32 scans at a resolution of 4 cm^{-1} to study the chemical structure of the rPET−GO membranes and the interaction between the polymer matrix and nanofillers. XRD (model X'Pert PRO, PANanalytical, The Netherlands), equipped with Cu Kα radiation (λ = 1.5406 Å), was used to study the microstructure of the prepared membranes and understand the distribution of GO sheets on the fiber surface. The crystallization and melting behaviors of the rPET/GO membranes were evaluated by using DSC (DSC-Q2000; TA Instruments, New Castle, USA). The thermal transitions, i.e., cold crystallization, melting, and crystallization from melt and their corresponding enthalpies (ΔH), were determined. Samples weighing approximately 5 mg first underwent cooling to −20 °C and then heated to 290 °C under a nitrogen atmosphere (at a flow rate of 25 mL min^{-1}). Both heating and cooling rates were kept the same at 10 °C min^{-1}, and the samples underwent three successive scans: heating, cooling, and heating. The analysis upon heating was conducted by using the second heating scan, while the cooling scan was used to evaluate the crystallization of polymers from the melt. Tensile tests were conducted according to the ASTM D882 standard to determine the modulus, yield strength, and elongation at break and were carried out using an Instron 5966 tensile tester (Instron Engineering Corporation, USA) equipped with a load cell of 10 kN at a constant rate of extension of 20 mm/min. The fiber mats were cut into rectangular strips of 95 × 25 mm sizes and mounted onto the tensile tester with the following dimensions: gauge length (L) = 40 mm and width (W) = 25 mm at 25 °C. Water contact angle (WCA) measurements were used to determine the surface wettability of the rPET/GO mats by using the sessile drop method. Membrane samples were placed on a platform, and droplets of 6−8 μL (DI water) were dropped carefully using a microsyringe on the membrane surface. A real-time camera captures the image of the droplet, and the CA is estimated.

AUTHOR INFORMATION

Corresponding Author

Suprakas Sinha Ray − *Centre for Nanostructures and Advanced Materials, DSI-CSIR Nanotechnology Innovation Centre, Council for Scientific and Industrial Research, Pretoria 0001, South Africa; Department of Chemical Sciences, University of Johannesburg, Johannesburg 2028, South Africa;* orcid.org/0000-0002-0007-2595; Email: rsuprakas@csir.co.za, ssinharay@uj.ac.za

Authors

Koena Selatile − *Centre for Nanostructures and Advanced Materials, DSI-CSIR Nanotechnology Innovation Centre, Council for Scientific and Industrial Research, Pretoria 0001, South Africa; Division of Polymer Technology, Department of Chemical, Metallurgical and Materials Engineering & Institute of Nanoengineering Research, Tshwane University of Technology, Pretoria 0001, South Africa*

Vincent Ojijo − *Centre for Nanostructures and Advanced Materials, DSI-CSIR Nanotechnology Innovation Centre, Council for Scientific and Industrial Research, Pretoria 0001, South Africa*

Rotimi Emmanuel Sadiku − *Division of Polymer Technology, Department of Chemical, Metallurgical and Materials Engineering & Institute of Nanoengineering Research, Tshwane University of Technology, Pretoria 0001, South Africa*

Complete contact information is available at: https://pubs.acs.org/10.1021/acsomega.1c02578

Notes

The authors declare no competing financial interest.

ACKNOWLEDGMENTS

The authors acknowledge the Department of Science and Innovation (HGERA8X), Council for Scientific and Industrial Research (HGER74P), and the University of Johannesburg (86310) for the financial support.

REFERENCES

(1) Chi, X.-Y.; Xia, B.-G.; Xu, Z.-L.; Zhang, M.-X. Impact of cross-linked chitosan sublayer structure on the performance of TFC FO PAN nanofiber membranes. *ACS Omega* **2018**, *3*, 13009−13019.

(2) Ahmed, F. E.; Lalia, B. S.; Hashaikeh, R. A review on electrospinning for membrane fabrication: Challenges and applications. *Desalination* **2015**, *356*, 15−30.

(3) Wang, Y.; Xu, T. Anchoring hydrophilic polymer in substrate: An easy approach for improving the performance of TFC FO membrane. *J. Membr. Sci.* **2015**, *476*, 330−339.

(4) Abdel-Mottaleb, M. M.; Khalil, A.; Karim, S.; Osman, T. A.; Khattab, A. High performance of PAN/GO-ZnO composite nanofibers for photocatalytic degradation under visible irradiation. *J. Mech. Behav. Biomed. Mater.* **2019**, *96*, 118−124.

(5) Mercante, L. A.; Scagion, V. P.; Migliorini, F. L.; Mattoso, L. H. C.; Correa, D. S. Electrospinning-based (bio)sensors for food and agricultural applications: A review. *TrAC, Trends Anal. Chem.* **2017**, *91*, 91−103.

(6) Makkam, S.; Harnnarongchai, W. Rheological and mechanical properties of recycled PET modified by reactive extrusion. *Energy Procedia* **2014**, *56*, 547−553.

(7) Seyyed Monfared Zanjani, J.; Saner Okan, B.; Menceloglu, Y. Manufacturing of multilayer graphene oxide/poly(ethylene terephthalate) nanocomposites with tunable crystallinity, chain orientations and thermal transitions. *Mater. Chem. Phys.* **2016**, *176*, 58−67.
(8) Strain, I. N.; Wu, Q.; Pourrahimi, A. M.; Hedenqvist, M. S.; Olsson, R. T.; Andersson, R. L. Electrospinning of recycled PET to generate tough mesomorphic fibre membranes for smoke filtration. *J. Mater. Chem. A* **2015**, *3*, 1632−1640.
(9) Chen, H.; Liu, Z.; Cebe, P. Chain confinement in electrospun nanofibers of PET with carbon nanotubes. *Polymer* **2009**, *50*, 872−880.
(10) Marcano, D. C.; Kosynkin, D. V.; Berlin, J. M.; Sinitskii, A.; Sun, Z.; Slesarev, A.; Alemany, L. B.; Lu, W.; Tour, J. M. Improved synthesis of graphene oxide. *ACS Nano* **2010**, *4*, 4806−4814.
(11) Istrate, O. M.; Paton, K. R.; Khan, U.; O'Neill, A.; Bell, A. P.; Coleman, J. N. Reinforcement in melt-processed polymer−graphene composites at extremely low graphene loading level. *Carbon* **2014**, *78*, 243−249.
(12) Dikin, D. A.; Stankovich, S.; Zimney, E. J.; Piner, R. D.; Dommett, G. H. B.; Evmenenko, G.; Nguyen, S. T.; Ruoff, R. S. Preparation and characterization of graphene oxide paper. *Nature* **2007**, *448*, 457−460.
(13) Park, H. S.; Choi, B. G.; Hong, W. H.; Jang, S.-Y. Controlled assembly of graphene oxide nanosheets within one-dimensional polymer nanostructure. *J. Colloid Interface Sci.* **2013**, *406*, 24−29.
(14) Al-Dhahebi, A. M.; Gopinath, S. C. B.; Saheed, M. S. M. Graphene impregnated electrospun nanofiber sensing materials: a comprehensive overview on bridging laboratory set-up to industry. *Nano Convergence* **2020**, *7*, 27.
(15) Huang, C.-L.; Wu, H.-H.; Jeng, Y.-C.; Liang, W.-Z. Electrospun graphene nanosheet-filled poly(trimethylene terephthalate) composite fibers: Effects of the graphene nanosheet content on morphologies, electrical conductivity, crystallization behavior, and mechanical properties. *Polymer* **2019**, *11*, 164.
(16) Yu, W.; Zhang, X.; Gao, X.; Liu, H.; Zhang, X. Fabrication of high-strength PET fibers modified with graphene oxide of varying lateral size. *J. Mater. Sci.* **2020**, *55*, 8940−8953.
(17) Jia, Y.; Chen, L.; Yu, H.; Zhang, Y.; Dong, F. Graphene oxide/polystyrene composite nanofibers on quartz crystal microbalance electrode for the ammonia detection. *RSC Adv.* **2015**, *5*, 40620−40627.
(18) Ramazani, S.; Karimi, M. Electrospinning of poly(ε-caprolactone) solutions containing graphene oxide: Effects of graphene oxide content and oxidation level. *Polym. Compos.* **2016**, *37*, 131−140.
(19) Lee, J.; Yoon, J.; Kim, J.-H.; Lee, T.; Byun, H. Electrospun PAN−GO composite nanofibers as water purification membranes. *J. Appl. Polym. Sci.* **2018**, *135*, 45858.
(20) Ramazani, S.; Karimi, M. Aligned poly(ε-caprolactone)/graphene oxide and reduced graphene oxide nanocomposite nanofibers: Morphological, mechanical and structural properties. *Mater. Sci. Eng. C* **2015**, *56*, 325−334.
(21) Botlhoko, O. J.; Ramontja, J.; Ray, S. S. Thermal, mechanical, and rheological properties of graphite- and graphene oxide-filled biodegradable polylactide/poly(ε-caprolactone) blend composites. *J. Appl. Polym. Sci.* **2017**, *134*, 45373.
(22) Yang, X.; Shang, S.; Li, L. Layer-structured poly(vinyl alcohol)/graphene oxide nanocomposites with improved thermal and mechanical properties. *J. Appl. Polym. Sci.* **2011**, *120*, 1355−1360.
(23) Botlhoko, O. J.; Ramontja, J.; Ray, S. S. Morphological development and enhancement of thermal, mechanical, and electronic properties of thermally exfoliated graphene oxide-filled biodegradable polylactide/poly(ε-caprolactone) blend composites. *Polymer* **2018**, *139*, 188−200.
(24) Wan, C.; Chen, B. Reinforcement and interphase of polymer/graphene oxide nanocomposites. *J. Mater. Chem.* **2012**, *22*, 3637−3646.
(25) Koo, H. J.; Chang, G. S.; Kim, S. H.; Hahm, W. G.; Park, S. Y. Effects of recycling processes on physical, mechanical and degradation properties of PET yarns. *Fibers Polym.* **2013**, *14*, 2083−2087.
(26) Mack, J. J.; Viculis, L. M.; Ali, A.; Luoh, R.; Yang, G.; Hahn, H. T.; Ko, F. K.; Kaner, R. B. Graphite nanoplatelet reinforcement of electrospun polyacrylonitrile nanofibers. *Adv. Mater.* **2005**, *17*, 77−80.
(27) Shin, J. E.; Kim, H. W.; Yoo, B. M.; Park, H. B. Graphene oxide nanosheet-embedded crosslinked poly(ethylene oxide) hydrogel. *J. Appl. Polym. Sci.* **2018**, *135*, 45417.
(28) Ghasemi, A.; Imani, R.; Yousefzadeh, M.; Bonakdar, S.; Solouk, A.; Fakhrzadeh, H. Studying the potential application of electrospun polyethylene terephthalate/graphene oxide nanofibers as electroconductive cardiac patch. *Macromol. Mater. Eng.* **2019**, *304*, 1900187.
(29) Jiang, L.; Shen, X.-P.; Wu, J.-L.; Shen, K.-C. Preparation and characterization of graphene/poly(vinyl alcohol) nanocomposites. *J. Appl. Polym. Sci.* **2010**, *118*, 275−279.
(30) Verma, S.; Mungse, H. P.; Kumar, N.; Choudhary, S.; Jain, S. L.; Sain, B.; Khatri, O. P. Graphene oxide: an efficient and reusable carbocatalyst for aza-Michael addition of amines to activated alkenes. *Chem. Commun.* **2011**, *47*, 12673−12675.
(31) Ganesh, B. M.; Isloor, A. M.; Ismail, A. F. Enhanced hydrophilicity and salt rejection study of graphene oxide-polysulfone mixed matrix membrane. *Desalination* **2013**, *313*, 199−207.
(32) Santos, R. P. O.; Rodrigues, B. V. M.; Ramires, E. C.; Ruvolo-Filho, A. C.; Frollini, E. Bio-based materials from the electrospinning of lignocellulosic sisal fibers and recycled PET. *Ind. Crops. Prod.* **2015**, *72*, 69−76.
(33) Huang, Y.-L.; Baji, A.; Tien, H.-W.; Yang, Y.-K.; Yang, S.-Y.; Ma, C.-C. M.; Liu, H.-Y.; Mai, Y.-W.; Wang, N.-H. Self-assembly of graphene onto electrospun polyamide 66 nanofibers as transparent conductive thin films. *Nanotechnology* **2011**, *22*, 475603.
(34) McKee, M. G.; Wilkes, G. L.; Colby, R. H.; Long, T. E. Correlations of solution rheology with electrospun fiber formation of linear and branched polyesters. *Macromolecules* **2004**, *37*, 1760−1767.
(35) Chae, D. W.; Kim, B. C. Effects of interface affinity on the rheological properties of zinc oxide nanoparticle-suspended polymer solutions. *Macromol. Res.* **2010**, *18*, 772−776.
(36) Lai, G. S.; Lau, W. J.; Goh, P. S.; Ismail, A. F.; Yusof, N.; Tan, Y. H. Graphene oxide incorporated thin film nanocomposite nanofiltration membrane for enhanced salt removal performance. *Desalination* **2016**, *387*, 14−24.

https://doi.org/10.1021/acsomega.1c02578
ACS Omega 2021, 6, 21005−21015